RESEARCH

RESEARCH: Review

On the origin of contact-electrification

Zhong Lin Wang [a,b,*], **Aurelia Chi Wang** [b,*]

[a] Beijing Institute of Nanoenergy and Nanosystems, Chinese Academy of Sciences, Beijing 100083, PR China
[b] School of Materials Science and Engineering, Georgia Institute of Technology, Atlanta, GA 30332, USA

Although contact electrification (triboelectrification) (CE) has been documented since 2600 years ago, its scientific understanding remains inconclusive, unclear, and un-unified. This paper reviews the updated progress for studying the fundamental mechanism of CE using Kelvin probe force microscopy for solid–solid cases. Our conclusion is that electron transfer is the dominant mechanism for CE between solid–solid pairs. Electron transfer occurs only when the interatomic distance between the two materials is shorter than the normal bonding length (typically ~0.2 nm) in the region of repulsive forces. A strong electron cloud overlap (or wave function overlap) between the two atoms/molecules in the repulsive region leads to electron transition between the atoms/molecules, owing to the reduced interatomic potential barrier. The role played by contact/friction force is to induce strong overlap between the electron clouds (or wave function in physics, bonding in chemistry). The electrostatic charges on the surfaces can be released from the surface by electron thermionic emission and/or photon excitation, so these electrostatic charges may not remain on the surface if sample temperature is higher than ~300–400 °C.

The electron transfer model could be extended to liquid–solid, liquid–gas and even liquid–liquid cases. As for the liquid–solid case, molecules in the liquid would have electron cloud overlap with the atoms on the solid surface at the very first contact with a virginal solid surface, and electron transfer is required in order to create the first layer of electrostatic charges on the solid surface. This step only occurs for the very first contact of the liquid with the solid. Then, ion transfer is the second step and is the dominant process thereafter, which is a redistribution of the ions in solution considering electrostatic interactions with the charged solid surface. This is proposed as a two-step formation process of the electric double layer (EDL) at the liquid–solid interface. Charge transfer in the liquid–gas case is believed to be due to electron transfer once a gas molecule strikes the liquid surface to induce the overlapping electron cloud under pressure. In general, electron transfer due to the overlapping electron cloud under mechanical force/pressure is proposed as the dominant mechanism for initiating CE between solids, liquids and gases. This study provides not only the first systematic understanding about the physics of CE, but also demonstrates that the triboelectric nanogenerator (TENG) is an effective method for studying the nature of CE between any materials.

＊ Corresponding authors at: Georgia Institute of Technology, Atlanta GA 30332, USA (Z.L. Wang and A.C. Wang).
  E-mail addresses: Wang, Z.L. (zhong.wang@mse.gatech.edu), Wang, A.C. (aurelia.wang0@gmail.com).

Phenomena of triboelectrification

Tribology is a highly complex process involving mechanical contacting/sliding of two materials, one against the other, in which many local physical and chemical processes occur, such as elastic/plastic deformations, fracturing, and generation of heat, as well as the presence of surface layers. Therefore, the study of tribology is primarily based on experimental observations, and there is no all-encompassing theory that can precisely predict tribology. However, tribology is a vitally important area for modern industries, transportation and construction despite being a challenge to quantitatively understand.

Triboelectrification (TE) is a united process of tribology and interfacial charge transfer, which is one of the most fundamental effects of electricity generation. The first well-recorded triboelectrification effect observed was lightning during thunderstorms (Fig. 1a). Under the heavy wind, contact between air molecules with water drops in air makes the water droplets negatively charged. The repulsion among the water droplets keeps them apart, but the fluctuation of local pressure and turbulence produced by the wind causes water droplets to recombine into larger water droplets, which will eventually form precipitation. With the decrease in surface area as a result of water droplet recombination, the surface charge density increases. Once the local electric field exceeds the air breakdown electric field, lightning will be produced. Here, a key question may be asked – why are the rain drops all negatively charged? A second well-known observation of TE appearing in textbooks is the rubbing of an animal's fur against a plastic rod (Fig. 1b). The stick will be negatively charged while the fabric will be positively charged, but thus far no one could explain why this occurs.

The scientific term for TE is contact electrification (CE), which means the charges are produced due to physical contact, and mechanical friction is not necessary although it can aid in delivering the charges. TE has been recorded since over 2600 years ago during ancient Greek civilization, and it exists everywhere, anywhere, and at any time, and despite this, this universal phenomenon that occurs for all known matter in solid, liquid, and even gas states is poorly understood. *Nature* published an article on triboelectric charging nearly a century ago, noting "This class of research is simple-seeming. But those who have spent time on the subject will allow that it is very baffling; those who have not done so will at least remember that despite great efforts by physicists the subject has not yet passed the pioneer stage" [1]. Now, 100 years later, this statement is still valid. Although TE is the most basic effect of electricity, studying the mechanisms of TE is rather cumbersome, possibly for the following reasons. First, TE is a very complex process that not only involves the basic processes occurring in tribology, but also interfacial charge exchange/tunneling. Secondly, the TE effect holds for all matter in solid, liquid, and gas states, so it is rather challenging to propose a unified physical model that covers such a broad range of materials. Thirdly, the lack of tools for probing nano-scale TE had been a major limitation for the field until the invention of Kelvin probe force microscopy (KPFM) based on the principle of atomic force microscopy (AFM) [2]. Even since then, there are only a few studies available in the literature using such a tool for this purpose. Lastly, TE is always regarded as a negative effect due to the fact that it can create electric fires and discharge, disrupted flow [3,4] and blending [5] in pharmaceutical processing, and leads to increased friction [6] and energy losses [7]. On the other hand, despite TE being the basis of the first technique used by ancient humans for creating fire for heating and cooking purposes through friction, there are few uses for TE in today's technology-based society aside from xerography, so why should funding and time be used to study this effect?
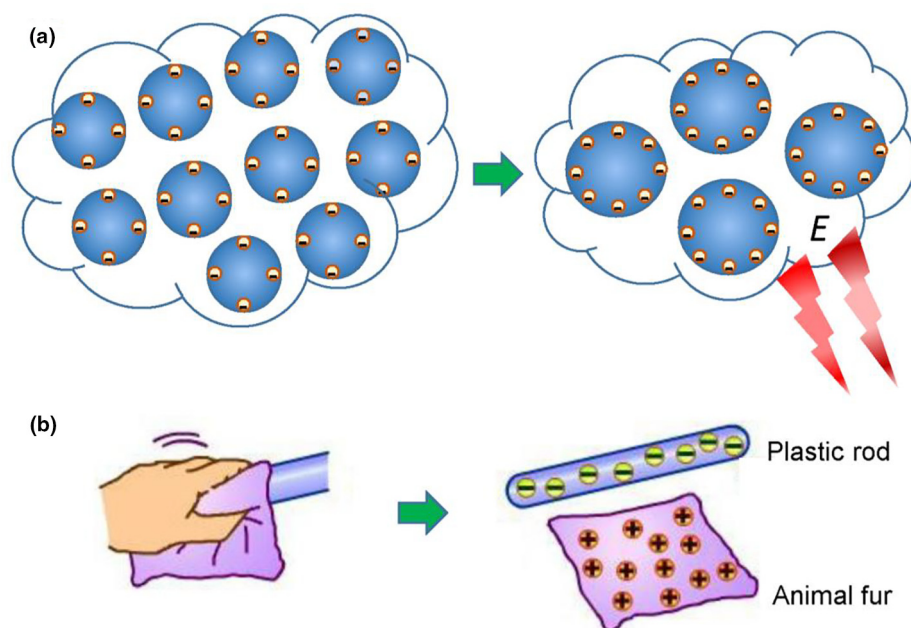

FIGURE 1

Schematic illustration regarding the formation of (a) thunderstorms and (b) basic triboelectrification examples that appear in physical science textbooks.

However, the situation has changed dramatically recently owing to the invention of triboelectric nanogenerators (TENGs) by Wang's group in 2012 [8,9]. The TENG is a fundamental technology for converting irregular, low-frequency, and distributed mechanical energy into electric power using a conjunction of triboelectrification and electrostatic induction. The area power density of TENGs has reached 500 W/m^2, the volume density has reached 490 kW/m^3, and a conversion efficiency of $\sim$50% has been demonstrated [10]. The TENG can be applied to harvest all kinds of mechanical energy that is ubiquitously available but wasted in our daily lives, such as human motion, walking, vibration, mechanical triggering, rotating tires, wind, flowing water and more, and thus has important applications in the internet of things and network of distributed energy [11]. Alternatively, the TENG can also be used as a self-powered sensor for actively detecting the static and dynamic processes arising from mechanical agitation using the voltage and current output signals of the TENG, respectively, with potential applications in robotics, soft/flexible electronics, and artificial intelligence. Networks of TENG units can be used for harvesting ocean water wave energy and general wind energy, with the possibility of contributing to worldwide energy production at large. TENGs use conventional materials that are low-cost, easy to fabricate, widely adaptable, and industrially scalable. Therefore, with the invention and future applications of TENGs, we have compelling reasons to study the fundamental science of TE, aimed at establishing the scientific basis of this new energy technology and largely improving its performance.

It has been proposed that TE is due to electron transfer [12], ion transfer [13–15] and/or even material's species transfer [16]. It was also suggested that H$^+$ and OH$^-$ ions from adsorbed water may transfer charges between surfaces [17]. Owing to the vast selection of materials that exhibit TE effects, there is hardly any convergence in scientific understanding of the nature of TE. The divergence in the field is similar to blind men touching an elephant, with each man's conclusion depending on which part of the elephant they touched. In this report, we systematically review the study of TE using KPFM and provide a uniform picture for understanding TE in systems of metal–dielectric and dielectric–dielectric cases. Our conclusion is that electron transfer is the dominant mechanism for TE among solids, liquids, and gases. Electron transfer occurs only when the interatomic separation between the two materials is forced to a shorter distance than the normal bonding length, which is the result of rubbing one material against another by applying an external force. A strong electron cloud overlap between the two atoms in the repulsive region leads to electron transition owing to the reduced interatomic potential barrier. The electrostatic charges on surfaces are released from the surface by thermal ionic emission and/or photon excitation. Some perspectives and predictions are given regarding new physics and analytical tools as a result of TE. This study not only provides the first systematic understanding of the physics of TE, which will be crucial for developing TENG-based energy and sensor technologies, but also demonstrates that the TENG is an effective tool for studying the nature of TE between any materials.

Through this and other reviews we have published, we intend to answer the following fundamental questions: (1) how are the electrostatic charges being created (the physics of CE); (2) how the electrostatic charges drive electrons to flow (the Maxwell's displacement current for TENG); (3) how the surface charge density being quantified; and (4) how do the current to be used for technologies (TENG).

Contact electrification in metal–dielectric cases

Rubbing a metal on a hard rock surface results in sparks and discharge, which is the result of triboelectrification in a metal–dielectric (M-D) case. By dielectric here and after, we means an insulator. Such a phenomenon has been known for centuries, but its nano-scale study using Kelvin probe microscopy (KPFM) was available only recently in the last few years. Shown in Fig. 2a is a case of scanning a Pt AFM tip on a SiO$_2$ surface in tapping mode. By repeatedly scanning over an area of about 5 μm in dimension, electrostatic charges are being delivered to the SiO$_2$ surface. The surface charge density reaches saturation after scanning about 8 times over (Fig. 2b) [18]. The line profile of the scanned region as provided by KPFM shows the potential distribution across the area, indicating that the surface has negative electrostatic charges (Fig. 2c).

The amount of charges delivered on the surface depends on the duration of tip contact [19]. In the tapping mode where the tip contacts the surface point by point, using a slow scan speed is more effective at delivering charges on surfaces (Fig. 3a). In the sliding mode where the tip continually contacts the surface, the charges are delivered effectively even at faster sliding speeds (Fig. 3b). This study indicates that sliding on and rubbing a surface with the tip is more effective in charging the surface in comparison to disjointed contact in the tapping mode (Fig. 3c and d). However, the surface charge density saturation limit remains the same value, regardless of whether the charges are delivered in tapping mode or contact mode, as long as the time spent in contact is long enough to reach that point (Fig. 3f). This is reasonable since the maximum limit to charge density that a surface can hold depends on the breakdown threshold of the surface in air.

The sign of the charges to be delivered on a dielectric surface can be manipulated by applying a bias voltage on the metal tip (Fig. 4a, b) [20]. By tuning the applied bias on the metal tip from −5 V to +5 V, the charges delivered to the surface changed from negative to positive, and there was no charge exchange observed when the applied bias was 3 to 4 V. The mechanism of CE in M-D cases can be well explained using an energy band diagram, in which the metal is characterized by its Fermi level, below which all of the states are occupied and above which, all of the states are empty (assuming the temperature is 0 K). The dielectric surface can be characterized using its conduction band (CB) and valence band (VB), but we must assume the presence of surface/defects states in the band gap due to the breaking of symmetry at the surface (Fig. 4c-i) [21]. If the edge of the valence band of the dielectric is below the Fermi level (E$_f$) of the metal, some of the surface states in the bandgap E$_g$ with energy below E$_f$ could be filled up by the electrons transferred from the metal into the dielectric, resulting in overall negative charges on the dielectric surface (Fig. 4c-ii) [22,23]. If a negative bias is applied on the metal tip (Fig. 4c-iii), the surface states on the dielectric side tend to be
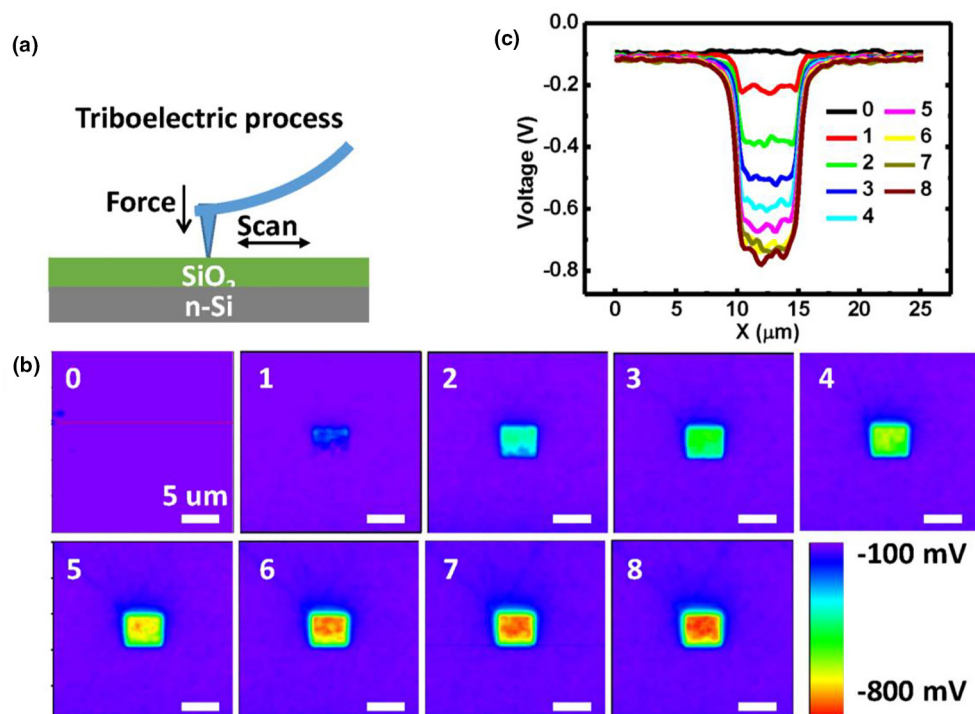
3

FIGURE 2

(a) Schematic of experimental setup of the AFM tip and the SKPM to map surface potential distribution. (b) Triboelectric charge accumulation on the SiO_2 surface with the increased counts of rubbing repetitions at the same area. Series of surface potential images taken in the same area from intact status to the one after the 8th rubbing cycle and (c) their corresponding potential profiles (With permission from ACS) [14].
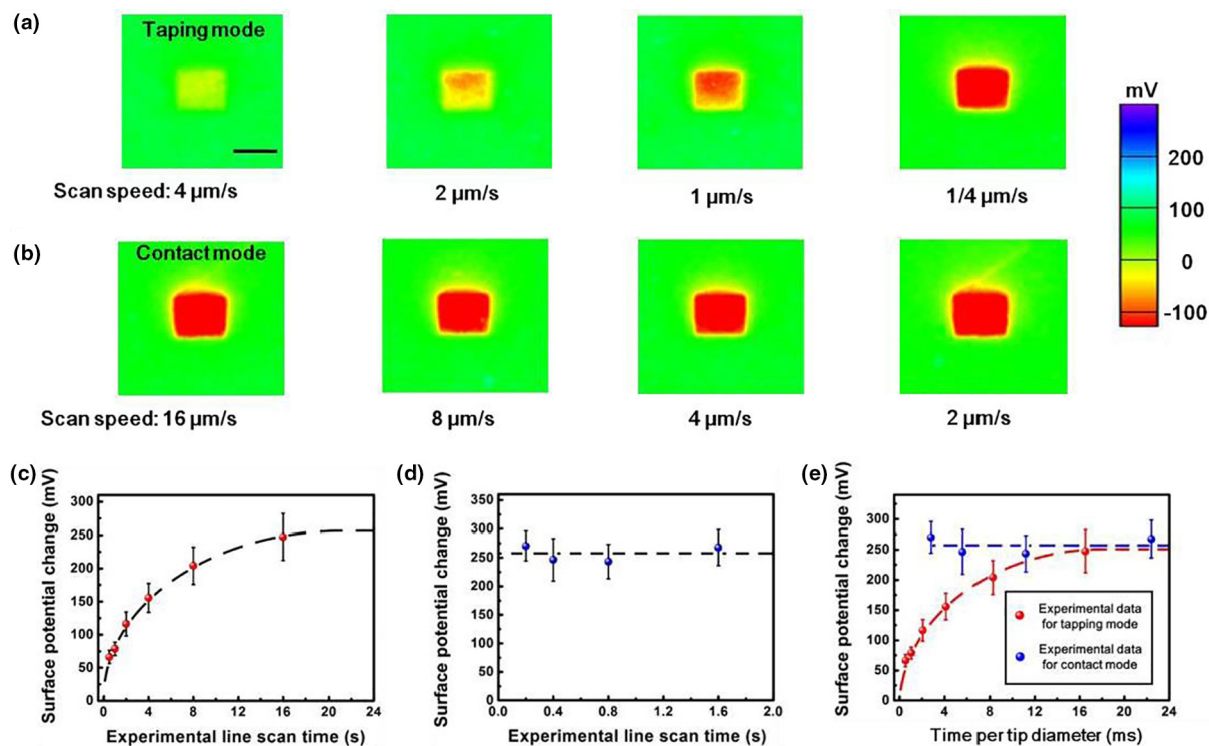

FIGURE 3

Comparison of electrostatic charge transfer dynamics between tapping mode and contact mode scans of an AFM tip. Surface potential mapping of parylene sample after the AFM probe scanned the central area at different scan speeds in (a) the tapping mode and (b) the contact mode. (c) and (d) Corresponding plots of surface potential change as functions of line scan time. (e) Comparison of the charge transfer density triggered by tapping mode and contact mode as a function of the tip–sample interaction time (with permission from Springer) [15].
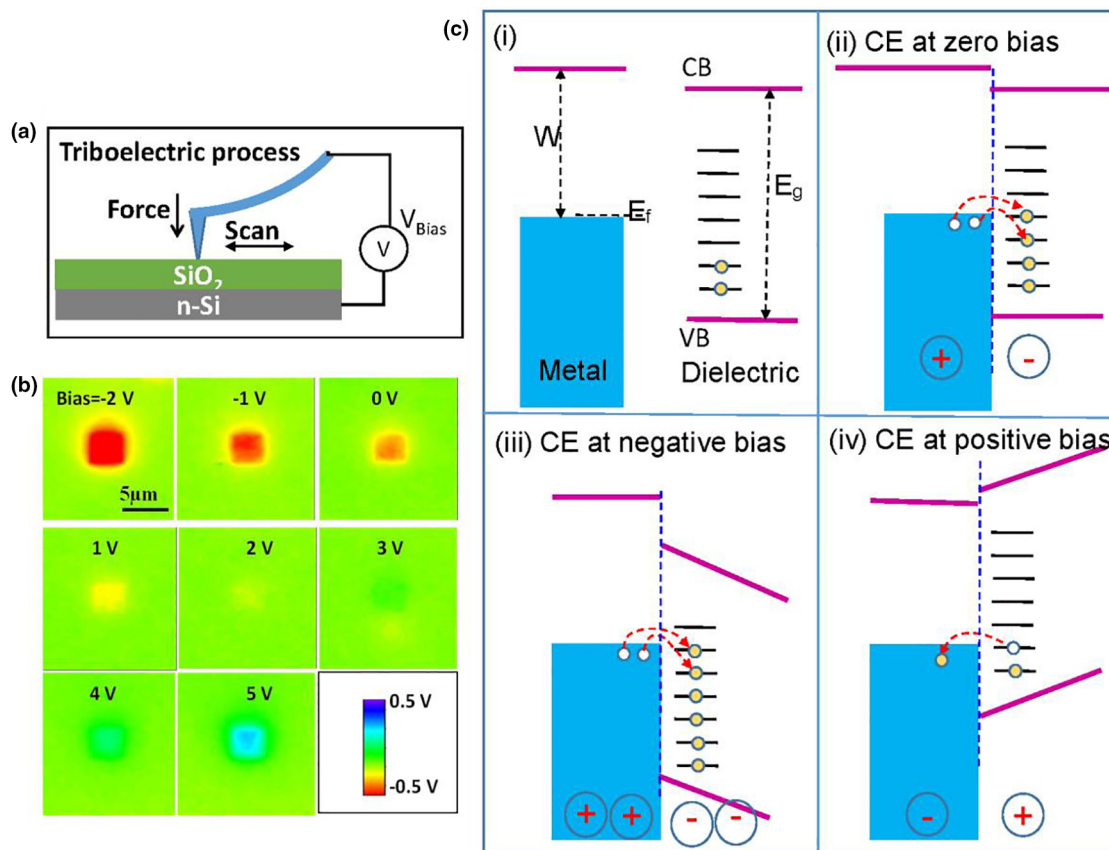
FIGURE 4

(a) Schematic of experimental setup of the AFM tip and the SKPM to map the surface potential distribution. (b) Surface potential distributions of the parylene film including the areas that were rubbed by the Pt-coated AFM tip at different bias from −2 to 5 V. (c) Schematic energy band diagrams for the metal and dielectric materials in the situations of precontact (i), in contact with no bias (ii), and in equilibrium with negative (iii) and positive (iv) bias (with permission from ACS) [18].

shifted to even lower energy levels in reference to the Fermi level of the metal, resulting in more electrons transferred from metal to dielectric. If a positive bias is applied (Fig. 4c-iv), the surface states in the dielectric side would be moved up to higher energy levels depending on the magnitude of the bias, and the electrons that occupy the surface states could be transferred to the metal, resulting in positive charges on the dielectric side. One can manipulate the magnitude of the applied bias in order to control the amount of charges to be transferred between a metal and dielectric. Studying of CE in metal–dielectric case has been around for a long time and it has been proposed that electron transfer is the dominant mechanism, and Kelvin probe force microscopy has provided nano-scale charge transfer information for these cases [24–27]. A recent AFM study also supports that CE in M-D cases is an electron transfer process [28]. The above discussion is valid if the electronic structure of the dielectric can be described by a band structure as we have presented, otherwise other models have to be adopted (see Section "Interatomic interaction model for general contact electrification cases").

Contact electrification in dielectric–dielectric cases

CE is a universal phenomenon that occurs for all materials, which is the challenge behind developing a unified picture to explain CE across the diverse spectrum of materials. For semiconductors and dielectric materials whose electronic structures can be represented by energy bands, CE between two materials can be easily presented as in Fig. 5 using the surface state model [29–32]. Considering the presence of surface and possibly point defects, surface or defect states exist in the bandgap. The presence of defects (surface defect structures) could result in the occupation of surface states by electrons. Owing to the different valance band and conduction band structures of each material, the occupied surface states in material A could have higher energy than that of the unoccupied surface states of material B (Fig. 5a). Once the two materials physically contact, some of the electrons could transfer from material A's surface to the surface of material B, leading to CE. Such electrons will not transfer back to material A even after the two materials are separated, resulting in net positive electrostatic charges on material A and negative electrostatic charges on material B (Fig. 5b). Such charges are surface-state-bound charges and cannot freely flow in general cases if the conductivity of the materials is rather low (e.g., insulators). Theoretically, these charges are expected to remain on surfaces perpetually if undisturbed. However, in the presence of thermal energy fluctuations and raised temperatures, these bound electrons can be released from surface states according to the thermionic emission model, which will be described in detail in Section "Effect of surface curvature on contact electrification of identical materials".
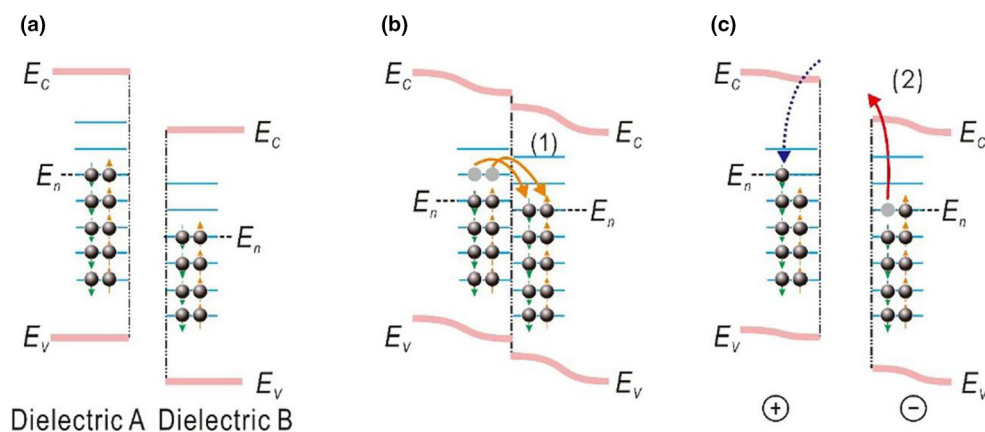
FIGURE 5

Charge transfer (a) before contact, (b) in contact, and (c) after contact between two different insulator dielectrics for a case that E_n of the former is higher than that of the latter and the band structure model holds (with permission from Wiley) [17].

Interatomic interaction model for general contact electrification cases

The discussions in Sections "Contact electrification in metal–dielectric cases" and "Contact electrification in dielectric–dielectric cases" are valid if the electronic structure of the dielectric can be represented by a band diagram with the presence of surface and defect states. As for general materials, such as polymers and rubbers, their electronic structures can be represented by molecular orbitals and chain alignment. An early review of observations can be found in [33]. On the other hand, for materials that may not have a well characterized molecular structure or in the presence of composite phases, as in natural materials, such as wool, wood, animal fur, and human hair, there is no simple electronic structure model that can represent these materials. We do know that all of these existing materials exhibit CE, and therefore a general model is needed for explaining CE on atomic and molecular levels [16].

We first start from experimental observations. The first question is: how close must the two atoms be before CE occurs? This question was answered by our study using KPFM [34]. Fig. 6 presents the surface potential difference (ΔV) between the center of the scanned area and the edge after a KPFM scan (Fig. 6a, c, e). Using amplitude-modulated (AM) AFM, the probe cantilever was excited near its resonance frequency (f_0), with a free vibration amplitude (A_0) set before the tip approaches the surface of the sample and a set-point scanning amplitude (A_{sp}) set as a feedback parameter to measure the topography of the sample surface after engagement. The interaction of the tip with the surface will extend or delay its vibration phase shift ($\Delta\varphi$) if there is an attractive or repulsive interaction between the two, respectively. By comparing the ΔV–A_{sp} and $\Delta\varphi$–A_{sp} curves of different A_0 (100, 70, and 50 nm), we explored the relationship between CE and the change of phase shift in the tapping mode. For the experiments of $A_0 = 100$ nm and $A_0 = 70$ nm, there are dramatic increases in ΔV from 0 (which means that contact electrification has had a significant influence on the surface potential) with A_{sp} being smaller than certain values ($\sim$95 nm for the experiment of $A_0 = 100$ and 62.5 nm for the experiment of $A_0 = 70$ nm), and

these values correspond to the sign switch point of the $\Delta\varphi$ in the $\Delta\varphi$–A_{sp} curves. In the case of $A_0 = 50$ nm, no CE was observed. Also, there is no decrease in the phase shift under such circumstances. When the tip has a net attractive force, it is in the attractive regime, and there is an increase in the phase shift ($\Delta\varphi > 0$). In contrast, if it has net repulsive force, it will be in the repulsive force regime, and there will be a decrease from the original phase shift ($\Delta\varphi < 0$). Therefore, the sign of $\Delta\varphi$ could be regarded as the symbol of the net tip–sample interaction force for each vibration cycle.

Accordingly, if the tip is in the attractive regime ($A_0 = 50$ nm), there is no electron transfer between the tip and sample. By increasing the free amplitudes ($A_0 = 70$ and 100 nm), the probe cantilever can vibrate with more energy. In this way, it could overcome the repulsive force and enter into the repulsive region. In this case, the tip is much closer to the surface of the sample in its lowest possible position (as shown in Fig. 6d, e). Since this tip–sample distance could result in tunneling, CE is observed in scanning experiments with $A_0 = 100$ and 70 nm (Fig. 6g). Moreover, since the A_{sp} for the transition between the attractive regime and the repulsive force regime is exactly the same value for the drastic increase in ΔV from 0 ($\sim$95 nm for the experiment of $A_0 = 100$ and 62.5 nm for $A_0 = 70$ nm), *the distance between the tip and the sample for electron transfer to occur should be smaller than the interatomic distance at equilibrium*, where the long range attractive force equals to the short-range repulsive force.

The repulsive and attraction interactions between atoms can be easily understood from the interatomic interaction potential. Fig. 7a shows the general representation of interatomic interactions. For two atoms that form a bond, which means some sort of overlap in electron clouds or wave function, an equilibrium distance a is established, which is called the bond length or interatomic distance. If the interatomic distance x is shorter than a, the two atoms tend to repel each other owing to the increased overlap of electron clouds (Fig. 7b). One of the key factors in CE is an external force that has to be applied in order for the two surfaces to be contacted. The role played by such an externally applied force is to create local high pressure at certain
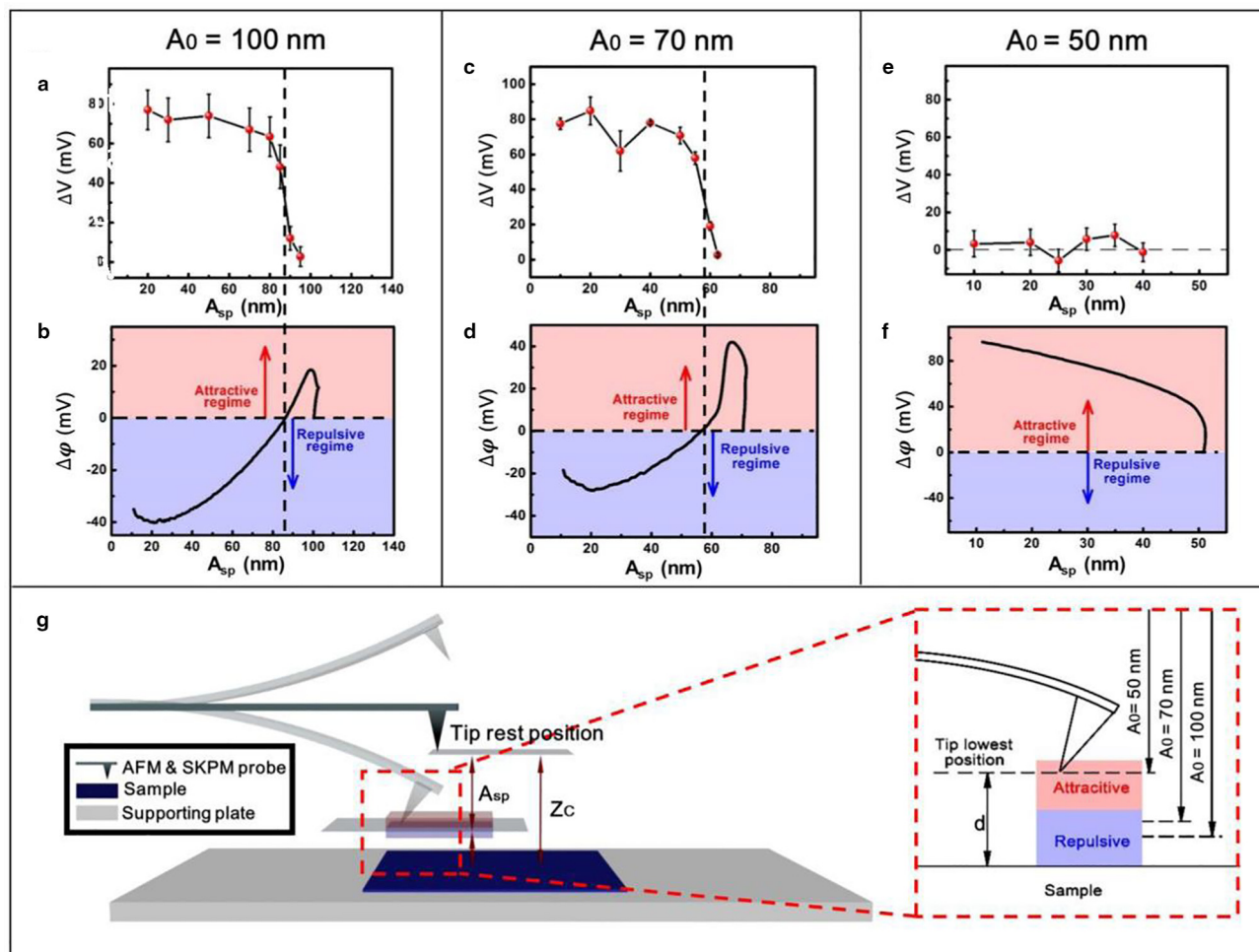
FIGURE 6

Exploring the relationship between contact electrification and the phase shift of the AFM cantilever in order to probe the force zone within which charge transfer occurs. (a–f) Surface potential difference ΔV–A_{sp} and $\Delta\varphi$–A_{sp} curves under the conditions of $A_0 = 100$, 70, and 50 nm. (g) Schematic of the tip-sample interaction force of tapping scans with different scanning parameters (A_0 and A_{sp}), as defined in (g). Whether the tip is in the attractive regime or repulsive regime above the surface of the sample can be deduced from the change of the phase shift ($\Delta\varphi$) during the tapping vibration (with permission from ACS) [18].
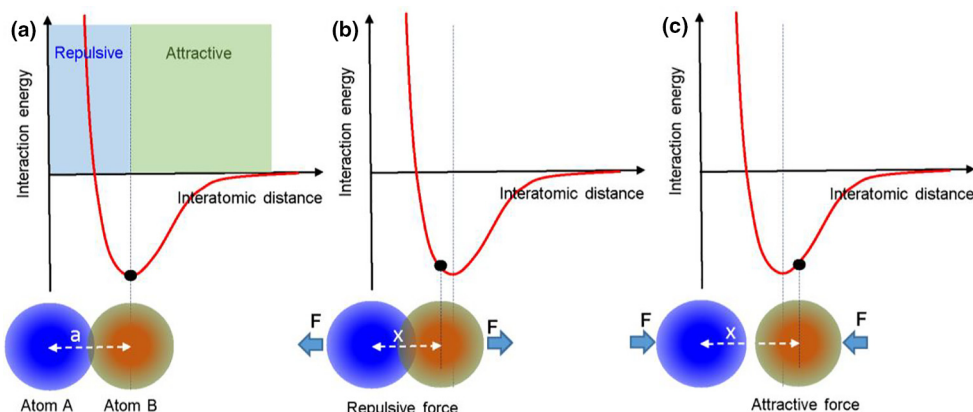

FIGURE 7

Interatomic interaction potential between two atoms and the force between the two when they are (a) at equilibrium position, (b) with strong electron cloud/wave-function overlap in the repulsive region, and (c) with little electron cloud/wave-function overlap in the attractive region.

contacting points even at atomic and nano-scales, where the interatomic distance x is forced to be shorter than a between the local contacting points, resulting in local repulsive force. If the interatomic distance x is larger than a, the two atoms tend to attract each other due to the reduced overlap of electron clouds, nearly breaking their bond (Fig. 7c).

The experimental results in Fig. 6 indicate that the distance between the AFM tip and the silica surface has to be shorter than the bonding length in order for the two to experience CE. In the repulsive region, the increased overlap in local electron clouds results in electron transition from one material to the other. Therefore, we can propose an atomic-scale charge transfer mechanism for CE [16,35]. Fig. 8a shows a case in which, prior to the atomic-scale contact of the two materials, their respective electron clouds remain separated without overlap. This is the attractive force region as presented in Fig. 8. The potential well binds the electrons tightly in specific orbitals and stops them from freely escaping, which is the case for non-conducting materials. When the two atoms belonging to two materials, respectively, get close to and contact with each other,

the electron clouds overlap between the two atoms to form an ionic or covalent bond. The bonding lengths are shortened even more if an external compression force is applied. In this case, the initial single potential wells become an asymmetric double-well potential, and the energy barrier between the two is lowered as a result of strong electron cloud overlap (Fig. 8b). Then electrons can then transfer from one atom to the other, resulting in CE. The role played by mechanical contact of the two materials is to shorten the distance between the atoms and cause a strong overlap of their electron clouds in the repulsive region, at least in the area at which the atomic-scale contact occurs, despite the samples being larger. It is important to note that only a very small fraction of area of the two surfaces will reach atomic scale contact. This also explains why more charges are transferred if one material rubs against the other harder/tighter owing to the strong compression force applied in sliding process, which can even cause local fractures and plastic deformation. After being separated (Fig. 8c), the transferred electrons remain as static charges on the material's surface.
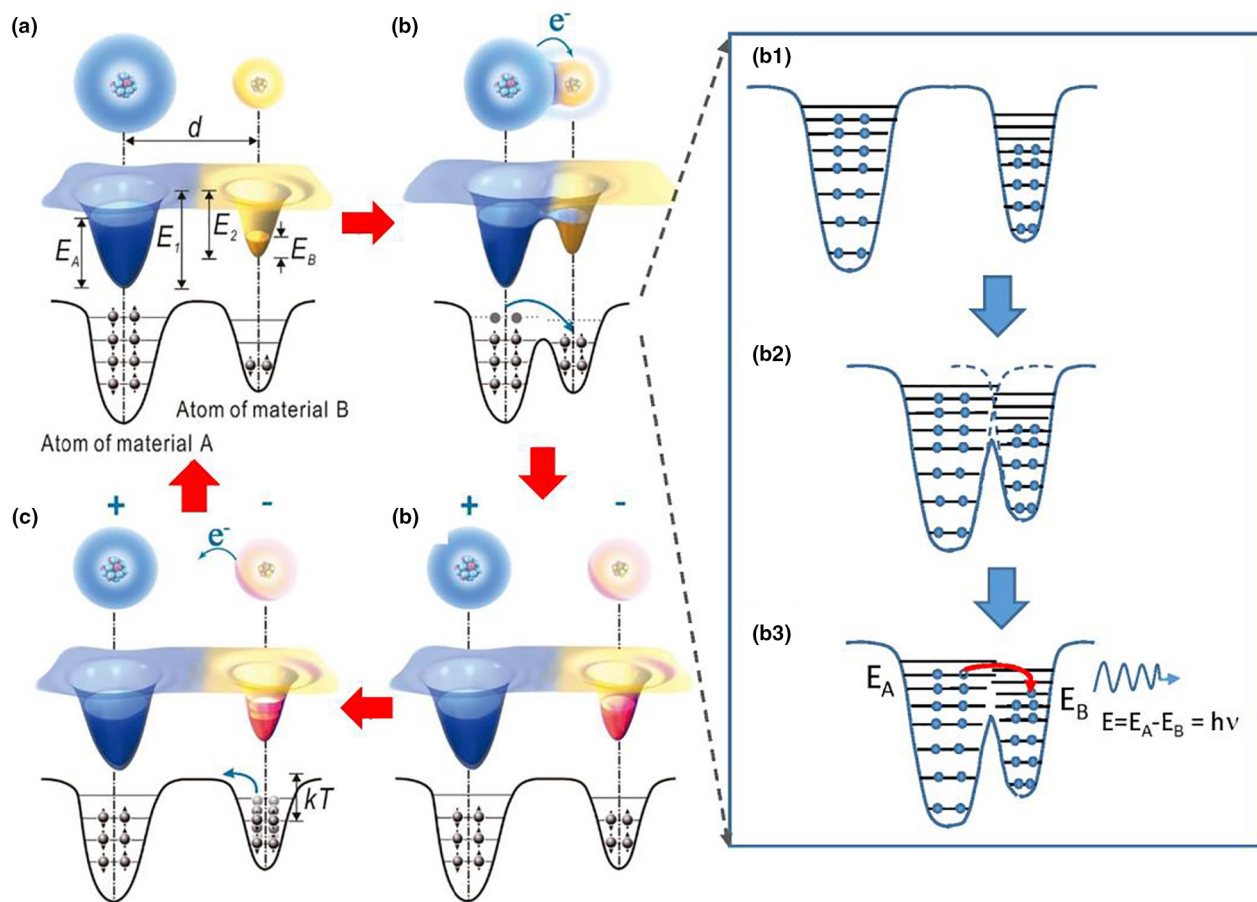

FIGURE 8

An electron-cloud-potential-well model proposed for explaining CE and charge transfer and release between two materials that may not have well-specified energy band structure, for general material cases. Schematic of the electron cloud and potential energy profile (3D and 2D) of two atoms belonging to two materials A and B, respectively, when they are: (a) before contact, (b) in contact, and (c) after contact, showing electron transfer from one atom to the other after being forced to have electron cloud overlap. (d) Charge release from the atom at an elevated temperature T once kT approaches the barrier height. d, distance between two nuclei; E_A and E_B, occupied energy levels of electrons; E_1 and E_2, potential energies for electrons to escape. (b1–b3) Detailed illustration of (b) to show that the increased electron cloud overlap results in a lower potential barrier between the two atoms, resulting in interatomic electron transition and possible photon emission (with permission from Wiley) [17].

The model proposed in Fig. 8 is also supported by quantum mechanical calculations, which state that the driving force for electrons to transfer is due to the delocalization of electron wave functions due to contact and strain [16,36–39], which is what we refer to as the state of strong overlap of electron clouds under stress. It is in this range that electron transfer is possible. The transition probability of an electron from one atom to the other as a function of the interatomic distance has been calculated [40], and the results support our discussion presented in Fig. 8.

Photon emission in contact electrification

Based on our model presented in Fig. 8, several photon emission processes are proposed [18]. According to Fig. 8b1–b3, energy released by electron transfer from dielectric A to dielectric B can be in the form of photon emission, plasmon excitation, and/or phonon excitation. Photon emission, if possible, can be used for studying the transition from the surface states of dielectric A to the surface states of dielectric B. The emitted photon should have energy in tens of eV, possibly resulting in UV, visible light, microwave, and even THz wave emission when two materials contact. The above proposed processes, if potentially observable as light emission, could give birth to a new optical spectroscopy for studying electronic transitions at interfaces. These results remain to be verified experimentally.

The energy of CE-produced electrons is not expected to exceed tens to hundreds of eV. By bombarding a metal plate using electrons emitted during peeling a piece of tape in vacuum, continuous X-rays with energies centered around 15 keV have been observed [41]. Considering the high electric field generated by CE charges, in the order of 10^5–10^6 V/m according to an AFM study [17], it is possible to generate a high voltage. Freely released electrons accelerated by such high voltages could result in strong X-ray radiation [42]. More study is needed in order to understand the observed phenomenon.

Effect of surface curvature on contact electrification of identical materials

It is generally known that physical contact of two dissimilar materials produces electrostatic charges, but experiments have shown that contact between two identical insulators also produces static charges [43–47]. In particulate materials, such as sand, smaller particles tend to be negatively charged and larger particles of the same material tend to be positively charged [48–50]. Such observations cannot be explained using either of the models we have proposed for dissimilar materials.

In order to understand the underlying mechanism in such cases, we have carried out detailed studies of the CE of two pieces of chemically identical materials that possess different curvatures, such as PTFE, Kapton, FEP, polyester, and nylon [51]. Polymers are chosen because we can change their curvature easily. By rationally designing materials with different surface curvatures, our results indicate that CE of two pieces of chemically identical materials results in concave surfaces being positively charged and convex surfaces being negatively charged (Fig. 9a–c). Our interpretation is that, owing to the fact that surfaces with different curvatures would have different surface energies possibly due to the stretched or compressed surface molecules, the energies

for specific surface states of the materials would be shifted considering the effects from surface energy (Fig. 9d). As a result, an electron can transfer from one material surface to another chemically identical surface with shifted surface states, once they physically contact (Fig. 9e). Furthermore, this means that the presence of a curved surface "breaks" the symmetry of the two sides, thus shifting the energy levels of surface states, resulting in electron transition, albeit with a smaller probability than dissimilar materials. The correlation of altered surface curvature with changes in surface energy is also supported by a theoretical study [52]. With considering a variation on surface morphology at the nano level and a rise of local temperature during probe scanning, mosaic surface charge distribution has been observed on surfaces [53].

Effect of temperature on contact electrification

In all of the existing literatures on triboelectrification, few studies are available about the temperature dependence of CE, as almost all of the measurements were made at room temperature. This lack of temperature dependence studies is potentially the basis of the confusion over whether charge transfer is due to electrons, ions or even materials species. We have recently studied the temperature dependence of CE, and our main conclusion is that electron transfer is the dominant, if not exclusive, mechanism for CE.

Transfer of charges across an interface

The temperature dependence of CE has been directly proved by scanning an Au tip on a SiO_2 surface (Fig. 10a) [54]. It is possible that the electrons would be thermally excited and transferred from the hotter material side to the cooler side. Hence, the charge transfer between the tip and the sample may be manipulated by setting the tip and sample to different temperatures. To verify this, the sample temperature was controlled at 373 K, while the SiO_2 sample temperature was varied from 313 K to 403 K. As shown in Fig. 10b, the transferred charge density increased linearly with rising tip temperature. When the tip temperature increased, the electrons in the tip were excited and more prone to hopping from the tip to the SiO_2 sample, and the sample became more negatively charged after contact.

The observed result can be explained using an energy band diagram, as shown in Fig. 10c [31]. Since the experiment was done at a temperature higher than 0 K, the distribution of electrons in the metal at different energies follows the Fermi–Dirac function:

$$f(E) = \frac{1}{e^{\left((E-E_f)/kT\right)} + 1} \tag{1}$$

where $f(E)$ denotes the probability of an electron in the energy level E, E_f denotes the Fermi level of the metal. Above the Fermi level, there is a tail filled with electrons.

In the first case, we assume that the Fermi level (E_f) of the metal is higher than the highest occupied surface state level (E_0) of the dielectric, and the metal tip temperature (T_m) is lower than the dielectric temperature (T_d) ($T_m < T_d$) (Fig. 10c-i), hence the energy increase in electrons in the metal ($\sim kT_m$) will be lower than the increase in electron energy in the dielectric ($\sim kT_d$). In this case, the electrons transfer from the metal to the dielectric
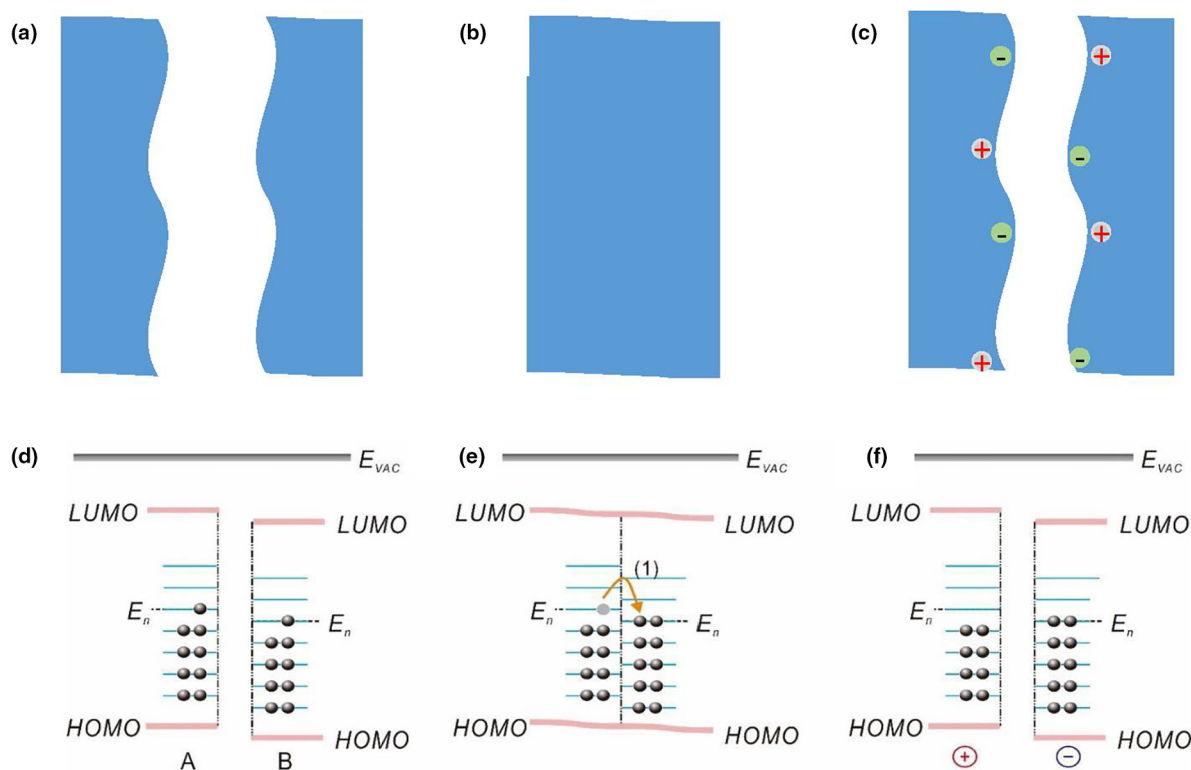
9

RESEARCH: Review

FIGURE 9

Mechanism of CE between identical polymer materials of different surface curvatures. (a–c) Charge transfer before contact, in contact, and after contact between identical material surfaces A and B with different surface curvatures, and (d–f) corresponding explanation of the surface charge transfer by the surface states model. LUMO, lowest unoccupied molecular orbital; E_n, neutral level of surface states; HOMO, highest occupied molecular orbital (with permission from ACS) [30].

in CE, as shown in Fig. 10c-ii. If the dielectric temperature is decreased while the metal temperature remains unchanged ($T_m = T_d$), as shown in Fig. 10c-iii, the energy increase in electrons in the metal ($\sim kT_m$) will be equal to the increase in electron energy in the dielectric ($\sim kT_d$). This leads to more electrons hopping from the metal to the dielectric than in the situation when $T_m < T_d$, as shown in Fig. 10c-iv. If the metal temperature is increased while the dielectric temperature remains unchanged ($T_m > T_d$), as shown in Fig. 11c-v, the increase in electron energy in the metal ($\sim kT_m$) will be higher than the increase in electron energy in the dielectric ($\sim kT_d$). This leads to more electrons hopping from the metal to the dielectric, as shown in Fig. 10c-vi. Since the dielectric temperature remains unchanged, the amount of electron tunneling back to the metal during surface separation remains nearly unchanged. Therefore, the triboelectric charges on the dielectric surface increase in this case.

The trend of CE is very much material dependent. By scanning an Au tip on aluminum nitride (AlN), the transferred charge density on the AlN surface was almost zero when the tip temperature was equal to the sample temperature (Fig. 11a). However, the AlN gained more negative charges from scanning when the tip temperature was higher than the sample temperature. The CE on Si_3N_4 experienced a sign reversal with an increase in tip temperature (Fig. 11b). The results show that, no matter if the transferred charges are positive or negative, more electrons are injected into the sample when the tip temperature is increased than when the

tip temperature equals the sample temperature. This is consistent with the thermionic electron emission model, in which the electrons in the tip are excited when the tip temperature increases and are more likely to transfer to the sample, making the triboelectric charges on the sample surface more negative.

In the second case, the Fermi level of the metal is lower than the highest occupied surface state level of the dielectric, and $T_m = T_d$, as shown in Fig. 11c-i. The electrons will transfer from the dielectric to the metal, and the dielectric will be positively charged, as shown in Fig. 11c-ii. When the metal temperature is increased, and the dielectric temperature remains unchanged ($T_m > T_d$), as shown in Fig. 11c-iii, the energy increase in electrons in the metal will be higher than the increase in electron energy in the dielectric. The gap between the effective Fermi level of the metal and the highest occupied surface state level of the dielectric becomes smaller, which leads to less electron hopping from the dielectric to the metal, and the dielectric receives fewer positive charges in CE, as shown in Fig. 11c-iv. In particular, if the metal temperature continues to increase and the dielectric temperature remains unchanged ($T_m \gg T_d$), the effective Fermi level of the metal will be higher than the highest occupied surface state level of the dielectric, as shown in Fig. 11c-v. In this case, the electrons will transfer from the metal to the dielectric, and the polarity of the transferred charges in the CE will be reversed (Fig. 11c-vi), as observed in the CE between the Au-coated tip and Si_3N_4.
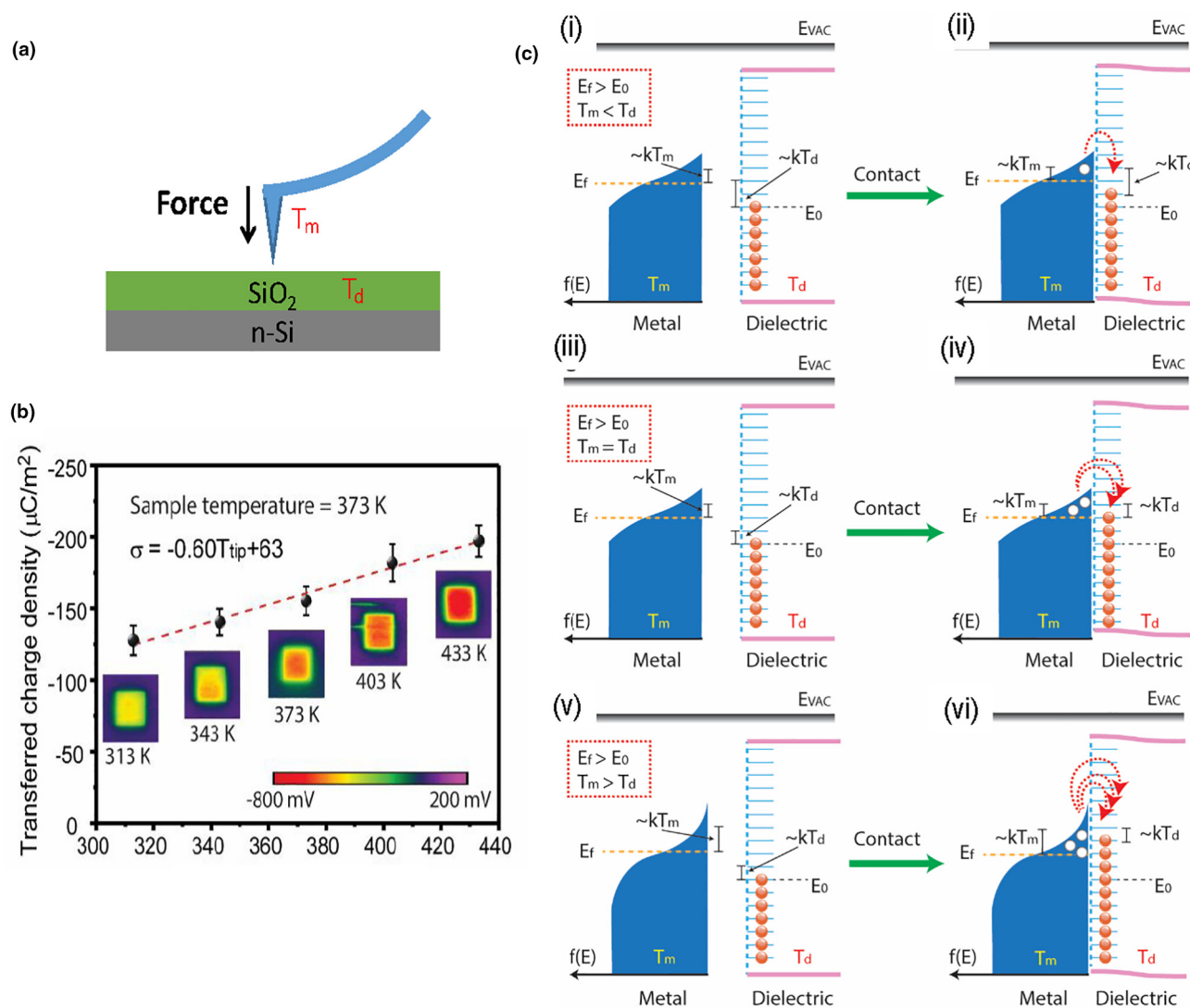
RESEARCH: Review

FIGURE 10

Proving the effect of temperature differences on CE between the Au-coated tip and the SiO$_2$ sample by KPFM at nano-scale. (a, b) The sample temperature was set at 373 K, while the tip temperature varied from 313 K to 433 K. (c) The band structure model of the temperature difference induced charge transfer ($E_f > E_0$). The band structure of the metal and surface states of the dielectric, when (i) the metal temperature is lower than the dielectric temperature, (iii) the metal temperature equals to the dielectric temperature, and (vi) the metal temperature is higher than the dielectric temperature. The illustration of contact charge transfer between the metal and the dielectric, when (ii) the metal temperature is lower than the dielectric temperature, (iv) the metal temperature equals to the dielectric temperature, and (v) the metal temperature is higher than the dielectric temperature (With permission from Wiley) [32].

Release of surface electrostatic charges

The TENG operates by coupling triboelectrification with electrostatic induction. The triboelectric field produces a driving force that makes electrons in the top and bottom metal electrodes flow due to the electrostatic induction effect. The measured total charges Q_{SC} flowing under the short circuit condition is a direct measure of the surface charge density, providing a new methodology for proving triboelectrification. Our TENG study has unearthed a surprising result: triboelectrification disappears at high temperature [16,18]. A TENG was constructed from thermally stable materials, such as Ti and SiO$_2$, as shown in Fig. 12a, so that the operating temperature could be uniformly increased. Fig. 12b shows the change of total output charges Q_{SC} of the TENG at temperatures of 353 K, 533 K and 583 K, demonstrating that the charge density decreased more

rapidly at higher temperatures. When the temperature reached 583 K, the charges quickly disappeared and the total Q_{SC} was less than 1 nC, similar to the disappearance of magnetism above the Curie temperature. Fig. 12c shows the residual charges on the TENG after 5 min of measurement at different temperatures, and the inset is the diagram of the Ti-SiO$_2$ TENG. The residual charges decreased more rapidly with the increase in temperature, and it is interesting to note that they started to decrease more rapidly once the temperature was higher than 533 K. Fig. 12d shows long-term charge decay under high temperatures, which indicates that increased temperatures lead to charge decay.

By quantitatively comparing the charge dissipation curve as a function of temperature, we concluded that the release of charges is best described by the thermionic electron emission
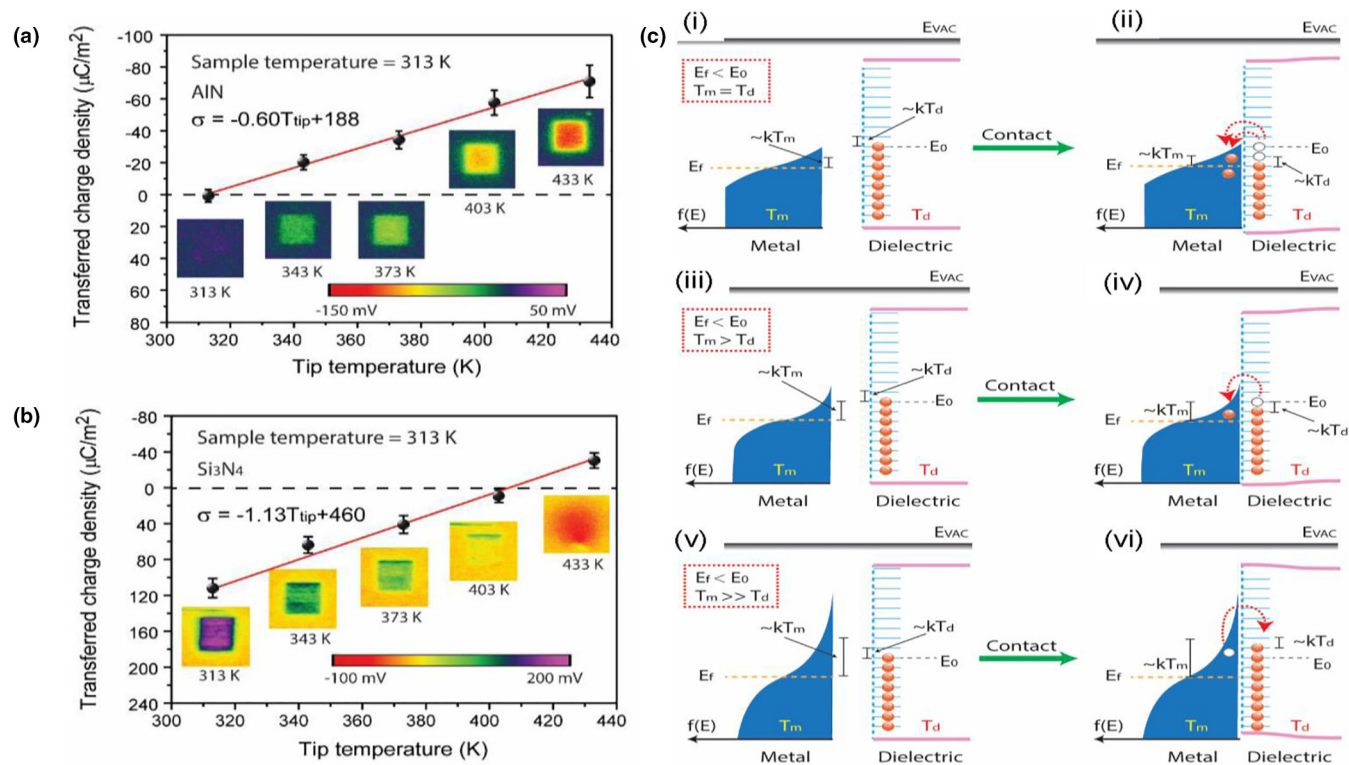
FIGURE 11

Proving the effect of temperature difference on the CE between an Au-coated tip and AlN and Si$_3$N$_4$ sample by KPFM at nano-scale. The relationship between transferred charge density on the (a) AlN, and (b) Si$_3$N$_4$ surfaces and the tip temperature when the sample temperature is maintained at 313 K. (c) The band-structure model of the temperature-difference induced charge transfer ($E_f < E_0$). (i, iii, v) The band structure of the metal and surface states of the dielectric, when the metal temperature equals the dielectric temperature, the metal temperature is higher than the dielectric temperature, and the metal temperature is much higher than the dielectric temperature, respectively. (ii, iv, vi) Illustrations of the contact charge transfer between the metal and the dielectric, when the metal temperature equals the dielectric temperature, the metal temperature is higher than the dielectric temperature, and the metal temperature is much higher than the dielectric temperature (With permission from Wiley) [32].

model, and the measured Q_{SC} values may be fitted according to the thermionic emission equation [55,56]:

$$J = \lambda A_0 T^2 e^{\frac{-W}{kT}} \left[e^{\frac{\Delta W}{kT}} - 1 \right] \tag{2}$$

where J is the current density, λ is the material-specific correction factor, A_0 is Richardson's constant of a free electron, T is temperature, W is the height of the potential barrier, k is Boltzmann's constant and ΔW is the potential barrier height variation due to the surface electric field E. When $\Delta W << kT$, the emission current density is related to the total transferred charges in a TENG by [16]

$$J \approx \frac{\lambda_1 A_0}{k} T e^{\frac{-W}{kT}} Q_{SC} \tag{3}$$

or equivalently:

$$\ln\left(\frac{J}{A_0 T}\right) = -\frac{W}{kT} + \ln\left(\frac{\lambda_1}{k} Q_{SC}\right) \tag{4}$$

Data simulation using Eq. (4) fits the experimental data well. Therefore, the dissipation of the charges on the surface follows the electron thermionic emission model.

Effect of photon excitation on contact electrification

Surface electrostatic charges can be released under photon excitation [57]. This process has been investigated by illuminating an insulator surface with light at a specific wavelength and inten-

sity. A requirement is to maintain that there is no significant change in surface temperature during the KPFM measurement, so that temperature effects can be ruled out. As shown in Fig. 13a, the triboelectric charges on the insulator surface were generated using the peakforce tapping mode, in which the tip contacts the insulator surface in a point by point "dancing" mode. After the CE, the triboelectric charge density on the insulator surface was measured using the KPFM mode. Furthermore, the charged area on the insulator surface was irradiated by UV light, and the triboelectric charge density remaining on the surface was measured at regular time intervals to record the charge decay.

In order to further verify the photoelectron emission of electrons in CE, the effects of light wavelength and intensity on the irradiation induced triboelectric charge decay were studied. Fig. 13b shows the effect of the incident light wavelength on the decay of triboelectric charges from the SiO$_2$ surface [34]. The charge decay rate was fastest when the wavelength was 240 nm, and the decay rate decreased with the increase in wavelength. In particular, the amount of the triboelectric charges remained constant when the wavelength rose up to 300 nm. The probability of the electrons, which were trapped in surface states following CE, being excited out of the surface was the largest under the irradiation of the light with a wavelength of
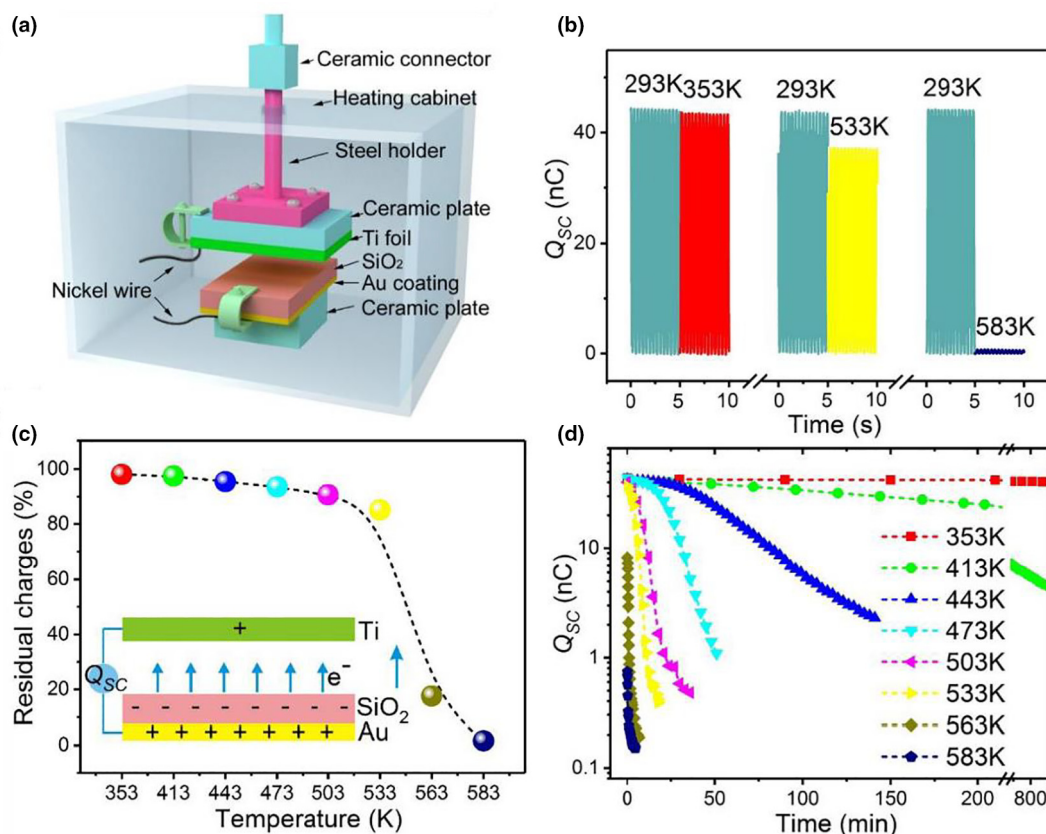
FIGURE 12

Probing the temperature dependence of the surface charge density in CE by using the output of a TENG, as a new method for quantitative analysis of CE. The TENG is made of a Ti and SiO_2 pair with metal electrodes at the top and bottom surfaces, respectively. (a) Setup of the measurement platform. (b) The total transferred changes Q_{SC} at room temperature and various high temperatures for three groups of experiments, respectively. (c) The percentage of residual charges of the TENG at different temperatures. The residual charges are the Q_{SC} of the TENG after 5 min heat preservation at different temperatures. Inset is the diagram of the working model of the TENG. (d) Q_{SC} evolution with time under high temperatures (with permission from Wiley) [17].

240 nm. When the light wavelength was increased, the energy of the photons and the probability of the electrons being excited would decrease, potentially leading to the decrease in the charge decay rate. When the light wavelength reached up to 300 nm, the energy of the photons was not enough to excite the trapped electrons, and the density of the triboelectric charge remained constant. The threshold energy of the incident photons should be higher than 4.13 eV to excite the electrons trapped in the surface states of SiO_2.

The UV light irradiation-induced triboelectric charge decay on polymer surfaces, such as PVC and PMMA, was also investigated [34]. Fig. 13c and 13d demonstrate the effects of light wavelength and intensity on the charge decay from the PVC surface. The triboelectric charge on the PVC surface could be removed by photons with wavelengths shorter than 360 nm (e.g., 3.44 eV). It means that the energy of photons required to remove charges on the PVC surface is less than that for the SiO_2 surface. The charge decay on the PVC surface was also linear at the beginning, and the decay rate decreased when the charge density decayed to less than a certain value. As shown in Fig. 13d, the charge decay rate on the PVC surface also increased with the rise of light intensity.

These studies show that there exists a threshold photon energy above which surface electrostatic charges will be released.

This has been explained by the photoelectron emission model. For the electrons trapped by surface states, a threshold energy is needed in order to excite an electron trapped in surface states into a free electron.

Standards and quantification of surface charge density

Triboelectrification is a well-known effect that occurs anywhere and anytime in nature and in our daily lives, but its quantification remains challenging. Although this effect has been known for over 2600 years and each and every material exhibits triboelectrification, as a key material's characteristic, its quantification has not been standardized and quantified in material science. The only available source commonly circulated in textbooks is a triboelectric series that gives a very inaccurate qualitative ranking of the triboelectric polarization of some common materials without numerical data. Quantification of CE is challenging due to the following aspects. First, since CE is a two-material problem, the performance of one material depends on its respective partner. Which material can be the reference partner material for all standardized measurements? Secondly, CE is a surface property, which is strongly affected by the roughness of the two surfaces, surface contamination, and atmospheric condi-
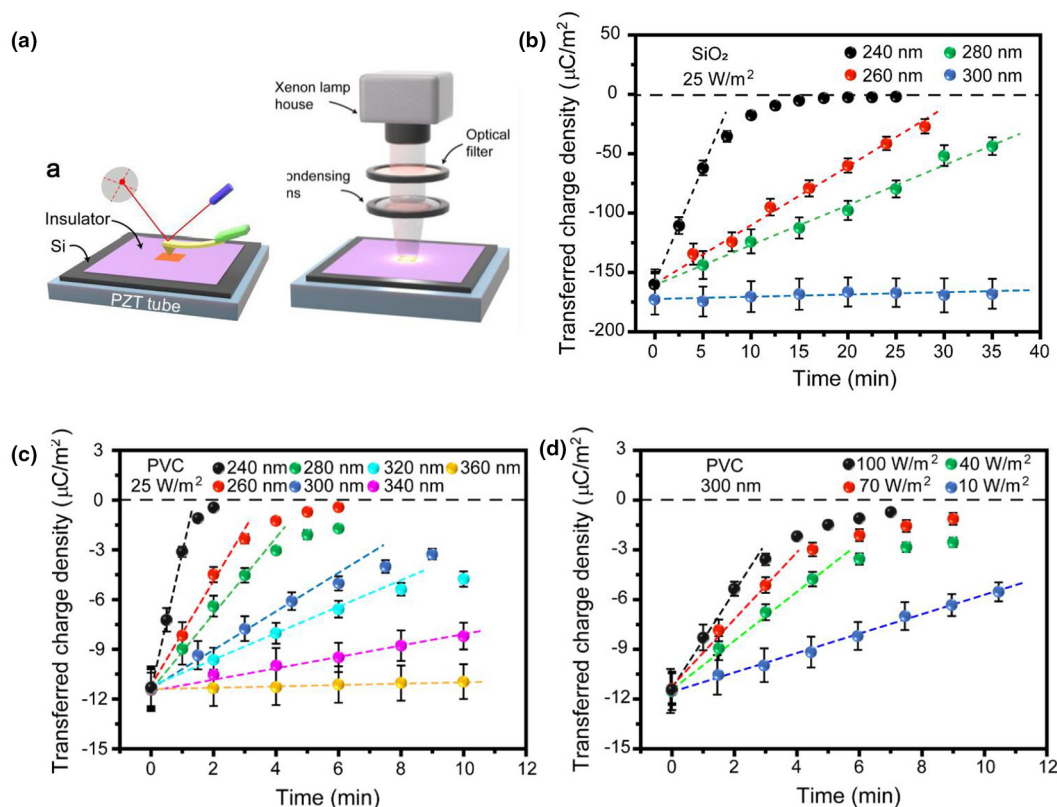
13

FIGURE 13

Probing the effect of photon excitation on the CE between an Au-coated tip and SiO$_2$ sample by KPFM at nano-scale. (a) Schematic illustration of the AFM and UV light irradiation experiments. (b) The effects of light wavelength on the charge decay on SiO$_2$ surface. The effects of (c) the light wavelength and (d) the light intensity on the charge decay on the PVC surface. In all of the experiments, careful measurements were made to ensure there was no significant increase in the sample temperature during the measurements (with permission from Wiley) [57].

tions, as well as humidity. A standardized method must be established to uniformly measure all of the materials, if possible.

We recently introduced a universal standard method to quantify the triboelectric series for a wide range of polymers, establishing a fundamental materials property of quantitative triboelectrification [58]. To maximize the contact of a material with the reference material, we chose liquid metal as the counter contact, which is likely to have the maximum atomic-scale contact, shape adaptability and softness. This method standardizes the experimental setup for uniformly quantifying the surface triboelectrification of general materials. The normalized triboelectric charge density (TECD) was defined and derived to reveal the intrinsic tendency of polymers to gain or lose electrons. A table is given regarding the TECD of over 50 materials (Fig. 14). This first quantitative triboelectric series will be a textbook standard for implementing the application of triboelectrification for energy harvesting and self-powered sensing. The methodology established will be extended to all conventional materials, such as ceramics, semiconductors, and polymers.

Discussion and summary
Electron transfer versus ion transfer in contact electrification
It has been long debated over whether CE is due to electron transfer, ion transfer, or even materials species transfer. First-principles' simulations [59] on surfaces of alumina and silica sup-

port the role of adsorbed water in surface charging: OH$-$ may be a dominant charge-carrying ion, through both surface transports, adsorption and desorption. OH$-$ ions are believed to accumulate at interfaces [60]. Studying CE at various elevated temperatures and photon excitations have clearly ruled out the contribution made by ion transfer, especially in solid–solid cases [17,37]. Firstly, the mechanism of releasing surface charges follows the electron thermionic emission model. Ion transfer satisfies the Boltzmann distribution [12], which indicates that more triboelectric charges would be transferred at higher temperatures, and this evidently disagrees with our experimental observations. Secondly, water plays a very important role in the ion transfer model [61], but fewer charges are transferred at higher moisture levels and maximum charge transfer has been found to occur at ∼0% relative humidity [62]. A recent study carried out triboelectric charging in oil, and showed that water is not necessary for contact electrification to occur [63]. Thirdly, CE between Ti and SiO$_2$ was observed even at 623 K, at which there are hardly any water-related ions remaining on solid surfaces [18]. Fourthly, studies by Wang et al. indicated that CE at a vacuum of 10^{-6} Torr was five times higher than that at one atmosphere pressure [64]. There are hardly any water molecules adsorbed on solid surfaces at such a high vacuum in comparison to ambient cases. Lastly, Liu et al. showed that a sustainable tunneling current had been produced using an unbiased, triboelectrically charged metal–insulator–semiconductor (MIS) point contact system [65]. All of these
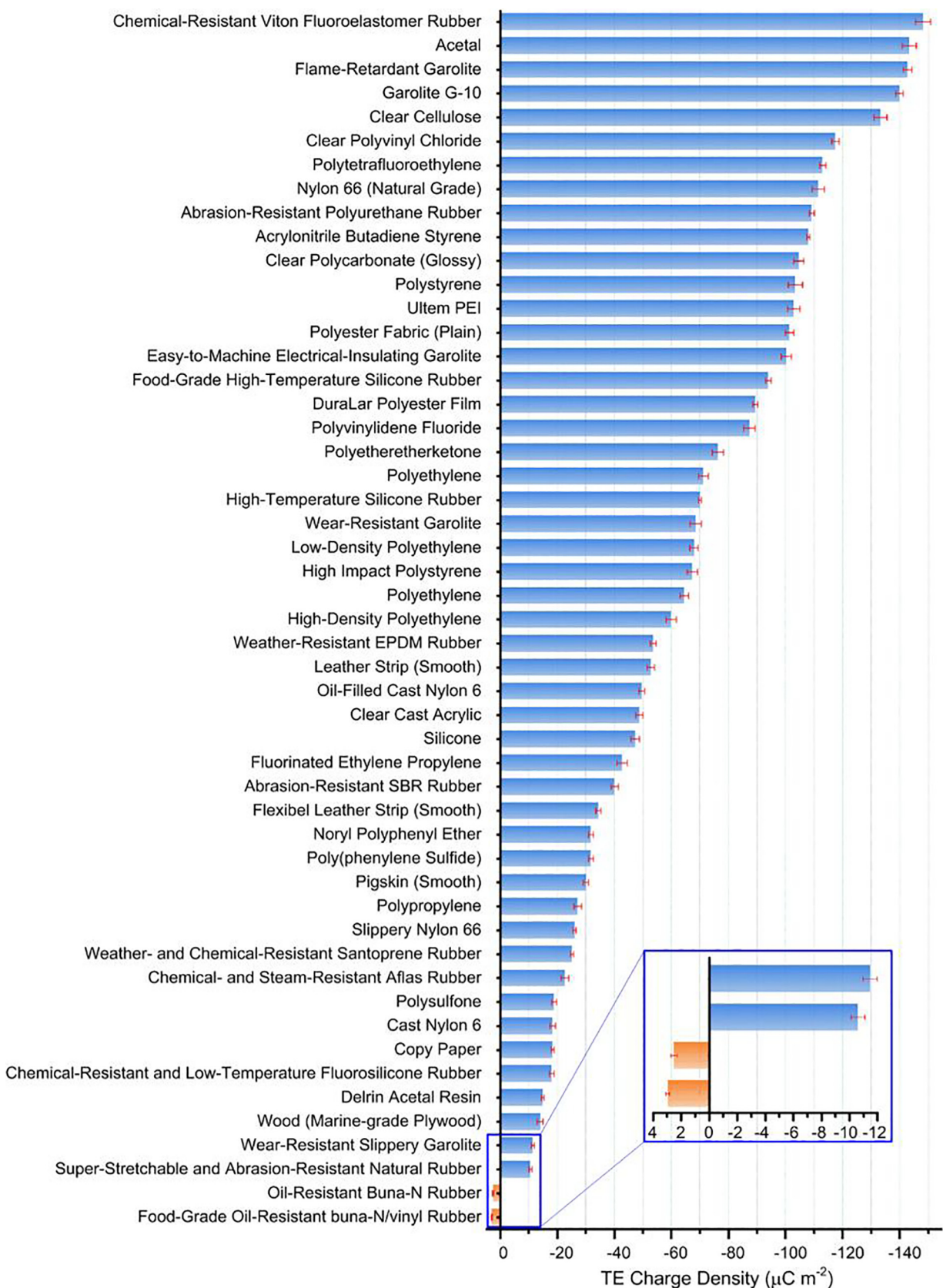
FIGURE 14

Quantified triboelectric series for over 50 different materials. The error bar indicates the range within a standard deviation (with permission from Nature) [58].

phenomena indicate that water ions are not necessary for CE, and the CE has to be an electron-dominated transition process.

Based on our studies, our conclusion is that CE is largely if not exclusively due to electron transfer. Electron transfer occurs if the interatomic distance is in the range of the repulsive force region, within which the electron clouds have maximized overlap. Surface discharge at elevated temperatures follows the electron thermionic emission model. The sign of the transferred charges in CE can be reversed by applying an electric field. Further studies found that the work required to separate the charged surfaces was comparable to the fracture energies of materials, which revealed that the electrification was associated with the interactions in electron clouds [66]. These studies indicate that the electrification is strongly related to electron transfer during the overlap of electron clouds, which further rule out the ion transfer mechanism. Finally, any contact between surfaces typically involves making and breaking of bonds, and CE is a consequence of such a process. Therefore, understanding of CE at the atomic- and nano-scale is fundamentally important for understanding bond formation and breaking between atoms.

A typical surface charge density related to triboelectrification can measure up to $\sim 10^{-3}$ C/m^2 in ambient condition, which corresponds to ~ 8 excess electrons per 10000 nm^2 of surface area. Thus, the probability of electron transfer is about one out of 30,000 surface atoms. Although this chance appears rather small, this charge transfer is an important quantum mechanical process that occurs in our lives at any place and any time.

Contact electrification at liquid–solid interfaces and the formation of EDL

CE occurs not only for solid–solid pairs but also at the interfaces between solids, liquids and gases, such as a raindrop with air in the liquid–gas case, sand particles with air in the solid–gas case, and at the solid–solution interface. A well-known phenomenon is the formation of an electrical double layer (EDL) at solid–liquid interfaces, which appears on the surface of an object when it is exposed to a liquid. The object might be a solid particle, a gas bubble, or a liquid droplet. The EDL refers to two parallel layers of charges surrounding the object. The first layer, the surface charge (either positive or negative), consists of ions adsorbed onto the object due to chemical interactions. The second layer is composed of ions attracted to the surface charges via the Coulomb force from the solution, electrically screening the first layer. This second layer is made of free ions that move in the liquid under the influence of electric attraction and thermal motion rather than being firmly anchored. Although the existence of EDL is a fact and its structure is clear, a fundamental question we would seek to ask is, what is the cause of the first layer becoming charged at the very beginning when it first contacts with a liquid? It might be related to the electron dominated CE at a very early stage of the object being exposed to a solution, as presented below.

The formation of the EDL is proposed as a two-step process. In the first step, when the molecules in the solution first approach a virgin surface that has no pre-existing surface charges (Fig. 15a), it may be possible that the atoms/molecules in the solution directly interact with the atoms on the solid surface to form strong overlap of electron clouds, as shown in Figs. 7 and 8. Elec-

tron transfer occurs first to make the "neutral" atoms on solid surface become charged, i.e., the formation of ions (Fig. 15b). For easy illustration, we label eight molecules as A–H, so one can easily follow the movements of the specific molecules at different stages. Under the pressure of the liquid flow or turbulence, the liquid molecules that are adjacent to the solid surface are thus forced/pushed off of the interface region by breaking the formed "bonds", leaving a layer of ions affixed to the solid surface (Fig. 15c) with the severed molecules becoming freely migrating ions in the liquid. It must be pointed out that the density of such surface charges should be comparable to the surface charge density in CE ($\sim$one out of 30,000 surface atoms, very sparsely distributed on the surface rather than the densely packed layers as depicted in many textbooks). In the second step, if there are ions existing in the liquid, such as H$^+$ and OH$^-$, the loosely distributed negative ions in the solution would be attracted to migrate toward the surface bonded ions due to electrostatic interactions, forming an EDL. The ζ potential is introduced to characterize the EDL. Our suggestion here is that the origin of forming the EDL is likely the result of CE due to electron transfer at the very first step. Once the EDL is formed, many discussions and models in the literatures regarding related potential distribution and surface chemistry are appropriate.

Contact electrification at liquid–gas and liquid–liquid interfaces

The model presented in Figs. 7 and 8 can also be applied to explain the CE between gas and a liquid. A well-known case is the friction between air molecules with water droplets to make charged raindrops. The water droplet is negatively charged due to the electron transfer from air molecules to the water droplet when the molecules strike the liquid surface. The charged molecules in a water droplet are loosely bound and free to move, and the charged air molecules tend to fly off the surface due to blowing of air and bombardment by other molecules. Thus, the total raindrop is negatively charged once it precipitates and falls through air.

By the same token, CE between liquid–liquid pairs should also exist. By compressing the molecules of one type of liquid against the surface of another liquid, the interface between the two is expected to be charged if they are immiscible, as a result of electron transfer. However, studies of this line of research are few.

Contact electrification at the interface of p- and n-type semiconductors

CE as for conventional materials can also occur for p- and n-semiconductors. Since the width of the depletion region at a pn junction is typically around a few nm, but CE occurs only at the top one to two atomic layers. The surface states at the n-side are filled with electrons, and the surface states are occupied by holes. At the very interface, in reference to Fig. 5 for insulators, a transition of electrons from the surface states of n-side to the hole states at p-side is likely to occur, resulting in p side to be negatively charged due to CE, and n-side positively charged. The energy released by such a transition could excite electron-hole pairs at the pn interface, possibly resulting in an observable current flowing from p-side to the n-side in the
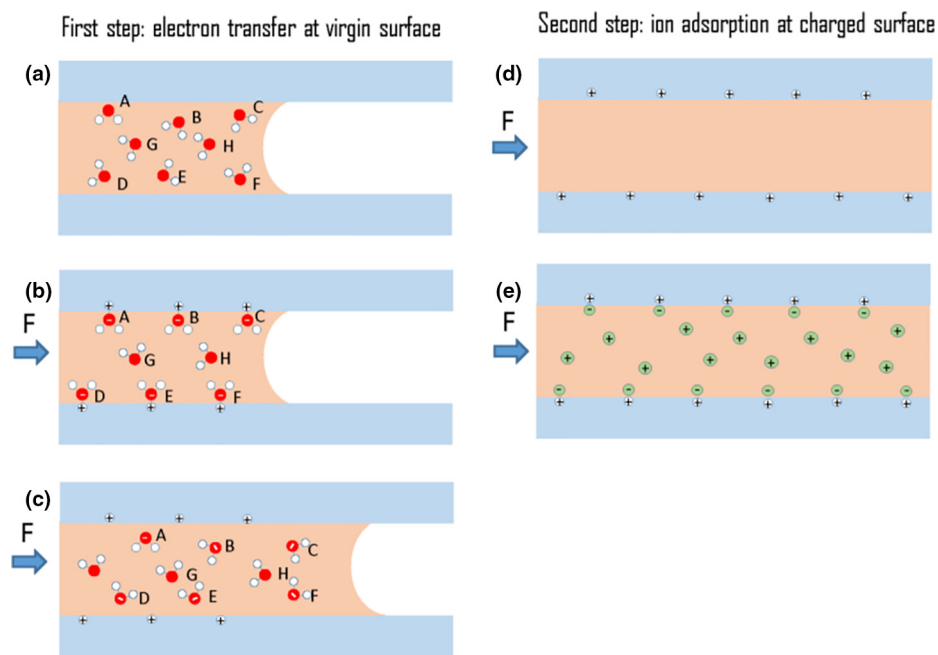
FIGURE 15

A proposed two-step model on the procedures for forming an electric double layer at a liquid–solid interface. The first step: formation of the very first layer of electrostatic charges on the solid surface. (a) Schematic representation of molecules in solution; (b) the adsorption of molecules on the surface and electron transfer, resulting in the surface being charged; and (c) the adsorbed molecules being pushed off the adsorbed locations due to the pressure of the liquid. The second step: segregation of ions in the liquid: (d) the presence of the charged surface as a result of the first step and (e) adsorption of ions in liquid on charged solid surface, forming the EDL.

external circuit, similar to photovoltaic effect. This may be simply referred to as the tribovoltaic effect.

By contacting a piece of p-type Si and an n-type Si wafer, an non-symmetric AC current has been observed in the external circuit [67], with a large current observed when the two pieces are separated apart and a smaller current is received when the two pieces are contacted with each other. This observed AC signal was interpreted as a result of difference in chemical potential as a result of redistribution of electric carriers. Here, we suggest that the current flowing from n-side to p-side when the n and p semiconductors are separated apart is likely due to carrier redistribution as suggested by Zhang et al., and the current flowing from p-side to n-side when the n and p semiconductors are contacted is possibly due to the tribovoltaic effect as discussed above, because CE is unavoidable when two materials are contacted. There are only limited studies available on the CE at a pn junction.

Alternatively, by sliding a n-semiconductor on top of a p-semiconductor without changing the current area (so called dynamic pn junction), the DC current observed by Lin et al. [68] is likely due to the tribovoltaic effect proposed above. Extensively studies are being carried out to verify the detailed mechanism of CE for semiconductor systems.

Advances in fundamental sciences and perspectives
We believe that we have answered the following fundamental questions related to electricity:

(1) How are the electrostatic charges being created?
This question is answered by the contents reviewed in this paper about CE, which should provide a fundamental understanding about how the electrostatic charges are created. We hope that an open question for over 2600 years has been answered.

(2) How do the electrostatic charges drive electrons to flow?
One way of outputting power using electrostatic charges is the TENG, which is governed by the Maxwell displacement current covered elsewhere [69,70]. The displacement current is created by coupling CE and electrostatic induction, so that electrons in metal electrodes are driven to flow under the mechanical triggering. This is the process of how the electric power is generated due to electrostatic interaction.

(3) How is the surface charge density quantified and calibrated?
This is answered in Section "Standards and quantification of surface charge density".

(4) How is the current used for technologies?
This is the basic technological application of TENG in fields like health care, environmental science, wearable electronics, internet of things, robotics, and artificial intelligence. Comprehensive review on TENG can be found elsewhere [9–11].

In summary, although CE has been known for 2600 years, longer than any recorded effect in science, its understanding remains premature. This paper reviews the updated progress in studying the fundamental mechanism of CE. Our main conclusion is that electron transfer is the dominant, if not exclusive, mechanism for CE. Ion transfer is a result of electron transfer at the very beginning, such as in the formation of the EDL at solid–liquid interfaces. Electron transfer due to overlapped

RESEARCH: Review

electron clouds under mechanical force is proposed as the dominant mechanism for CE between solids, liquids, and gases. The motivation behind studying CE is also to build high-performance TENGs, which has important applications as micro/nano-power sources, self-powered sensors, and blue energy. The energy and sensor technologies based on TENGs will significantly impact the development of the internet of things, wearable/flexible/stretchable electronics for medical science, robotics, and artificial intelligence.

Nie et al. [71] present a TENG that can work based on the interaction between two pure liquids. A liquid–liquid TENG is achieved by passing a liquid droplet through a freely suspended liquid membrane. This is a good example for studying charge transfer between liquid and liquid.

Xu et al. [72] have studied TENGs fabricated using Pt-Al_2O_3 TENG, Au-Al_2O_3 TENG, Ti-Al_2O_3 TENG, Al-Al_2O_3 TENG and SiO_2-Al_2O_3. The results show that the potential barrier of materials can be regulated by changing the contacting metals or dielectrics. It is mainly due to the work function or contact potential difference that have an influence on the propensity or direction of electron transfer between materials. Regulation of the barrier at high temperatures fully excludes the influence of ions from moisture and functional groups, which further indicates the dominant role played by electron transfer in CE.

Acknowledgments

References

[1] P.E. Shaw, Nature 118 (1926) 659–660.
[2] B.D. Terris et al., Phys. Rev. Lett. 63 (1989) 2669–2672.
[3] K.C. Pingali et al., Int. J. Pharm. 369 (2009) 2–4.
[4] F. Salama et al., J. Electrostat. 71 (2013) 21–27.
[5] Y. Pu, M. Mazumder, C. Cooney, J. Pharm. Sci. 98 (2009) 2412–2421.
[6] T.A.L. Burgo et al., Sci. Rep. 3 (2013) 2384.
[7] K. Sayfidinov et al., Sci. Adv. 4 (2018) eaau3808.
[8] F.R. Fan, Z.Q. Tian, Z.L. Wang, Nano Energy 1 (2012) 328–334.
[9] Z.L. Wang et al., Triboelectric Nanogenerators, Springer, 2016.
[10] Z.L. Wang, ACS Nano 7 (2013) 9533–9557.
[11] Z.L. Wang, J. Chen, L. Lin, Energy Environ. Sci. 8 (2015) 2250–2282.
[12] C.-Y. Liu, A.J. Bard, Chem. Phys. Lett. 480 (2009) 145–156.
[13] W.R. Harper, Contact and Frictional Electrification, Clarendon Press, Oxford, 1967.
[14] L.S. McCarty, G.M. Whitesides, Angew. Chem. Int. Ed. 47 (2008) 2188–2207.
[15] A.F. Diaz, D. Wollmann, D. Dreblow, Chem. Mater. 3 (1991) 997–999.
[16] J. Lowell, J. Phys. D: Appl. Phys. 10 (1977) L233.
[17] O. Knoblauch, Z. Phys Chem. 39 (1902) 225–244.
[18] Y.S. Zhou et al., Nano Lett. 13 (2013) 2771–2776.
[19] Y.S. Zhou et al., Nano Res. 9 (2016) 3705.
[20] Y.S. Zhou et al., Nano Lett. 14 (2014) 1567–1572.
[21] J. Lowell, A.R. Akande, J. Phys. D 21 (1988) 125–137.
[22] L.-H. Lee, J. Electrost. 32 (1994) 1–29.
[23] F.A. Vick, Br. J. Appl. Phys. 4 (1953) S1.
[24] S.-M. Huang, R.T. Atanasoski, R.A. Oriani, J. Electrochem. Soc. 140 (1993) 1065–1067.
[25] A. Verdaguer et al., Appl. Phys. Lett. 94 (2009) 233105.
[26] M.T. Nguyen et al., Langmuir 10 (1994) 597–601.
[27] H. Sun et al., Appl. Phys. Lett. 96 (2010) 083112.
[28] J. Liu et al., Nat. Nanotechnol. 13 (2018) 112.
[29] G.S.P. Castle, L.B. Schein, J. Electrost. 36 (1995) 165–173.
[30] G.S.P. Castle, J. Electrost. 40&41 (1997) 13–20.
[31] L.B. Schein, M.L. Ha, D. Novotny, Phys. Lett. A 167 (1992) 79–83.
[32] C. Xu et al., Adv. Mater. 30 (2018) 1706790.
[33] J. Fuhurmann, J. Electrost. 4 (1977) 109–118.
[34] S.M. Li et al., ACS Nano 10 (2016) 2528–2535.
[35] C. Xu et al., Adv. Mater. 30 (2018) 1803968.
[36] X. Shen et al., J. Electrostat. 82 (2016) 11–16.
[37] S.A. Lina, T.M. Shao, Phys. Chem. Chem. Phys. 19 (2017) 29418–29423.
[38] Y. Zhang, T. Shao, J. Phys. D: Appl. Phys. 46 (2013) 235304.
[39] C.B. Duke, T.J. Fabish, J. Appl. Phys. 49 (1978) 315–320.
[40] M. Willatzen, Z.L. Wang, Nano Energy 52 (2018) 517–523.
[41] H. Stöcker et al., J. Electrost. 71 (2013) 905–909.
[42] C.G. Camara et al., Nature 455 (2008) 1089.
[43] T. Shinbrot, T.S. Komatsu, Q. Zhao, Europhys. Lett. 83 (2008) 24004.
[44] M.M. Apodaca et al., Angew. Chem. Int. Ed. 49 (2010) 946–949.
[45] M.M. Apodaca et al., Angew. Chem. Int. Ed. 49 (2010) 946–949.
[46] R. Pham et al., J. Electrostat. 69 (2011) 456–460.
[47] J. Lowell, W.S. Truscott, J. Phys. D: Appl. Phys. 19 (1986) 1281–1298.
[48] H. Zhao et al., IEEE Trans. Indust. Appl. 39 (2003) 612–618.
[49] K.M. Forward, D.J. Lacks, R.M. Sankaran, Phys. Rev. Lett. 102 (2009) 028001.
[50] M.A. Bilici et al., Rev. Sci. Instr. 85 (2014) 103903.
[51] C. Xu et al., ACS Nano 13 (2019) 2034–2041.
[52] G. Makov, A. Nitran, Phys. Rev. B 47 (1993) 2301–2307.
[53] H.T. Baytekin et al., Science 333 (2011) 308–312.
[54] S.Q. Lin et al., Adv. Mater. (2019), https://doi.org/10.1002/adma.201808197.
[55] C. Crowell, Solid State Electron. 8 (1965) 395.
[56] J. Racko, A. Grmanová, J. Breza, Solid State Electron. 39 (1996) 391.
[57] S.Q. Lin et al., Adv. Mater (2019) 1901418, https://doi.org/10.1002/adma.201901418.
[58] H.Y. Zou et al., Nat. Commun. 10 (2019) 1427, https://doi.org/10.1038/s41467-019-09461-x.
[59] R. Fu, X. Shen, D.J. Lacks, J. Phys. Chem. C 121 (2017) 12345–12349.
[60] L.S. McCarty, A. Winkleman, G.M. Whitesides, Angew. Chem. Int. Ed. 46 (2007) 206–209.
[61] T.A. Burgo et al., J. Electrostat. 69 (2011) 401.
[62] V. Nguyen, R. Yang, Nano Energy 2 (2013) 604.
[63] H.T. Baytekin et al., Angew. Chem. Int. Ed. 50 (2011) 6766–6770.
[64] J. Wang et al., Nat. Commun. 8 (2017) 88.
[65] J. Liu et al., Nano energy 48 (2018) 320–326.
[66] R.G. Horn, D. Smith, Science 256 (1992) 362.
[67] Q. Zhang, R. Xu, W. Cai, Nano Energy 51 (2018) 698–703.
[68] Y. Lu, et al., arXiv preprint arXiv:1901.00701.
[69] Z.L. Wang, Materials Today 20 (2017) 74–82.
[70] Z.L. Wang, T. Jiang, L. Xu, Nano Energy 39 (2017) 9–23.
[71] J. Nie et al., Nature Communication 10 (2019) 2264, https://doi.org/10.1038/s41467-019-10232-x.
[72] C. Xu et al., Adv. Func. Mater., https://doi.org/10.1002/adfm.201903142.